Effects of Alloying Elements on Impact Properties of Ultra High-Strength TRIP-Aided Bainitic Ferrite Steels

Tomohiko HOJO*, Junya KOBAYASHI**, Tomohiro KAJIYAMA** and Koh-ichi SUGIMOTO***

To improve the toughness of ultra high-strength steels, the effects of alloying elements on impact properties of ultra high-strength low alloy TRIP-aided steels with bainitic ferrite matrix (TBF steels) were investigated. In this study, C-Si-Mn and C-Si-Mn-Al-Nb-Mo TBF steels were used. Upper shelf Charpy impact absorbed value of TBF steels were changed by the austempering treatments after annealing. When aluminium, niobium and molybdenum were added to C-Si-Mn TBF steels, excellent Charpy impact absorbed values were achieved. These were caused by the existence of a large amount of stable retained austenite due to the aluminium addition. Fracture appearance transition temperature of TBF steel was lowered by aluminium, niobium and molybdenum combined addition. This was caused by refined bainitic ferrite matrix by the aluminium addition and fine grain size by the addition of niobium and molybdenum. Hydrogen embrittlement on Charpy impact absorbed value of TBF steel was suppressed. This was because that retained austenite absorbed a lot of hydrogen and suppressed the hydrogen trapping to the grain boundaries.

Key Words: *TRIP-aided steel, ultra high-strength steel, retained austenite, bainitic ferrite, toughness, alloying element, hydrogen*

1. INTRODUCTION

Recently, to reduce the weight and improve the impact safety of vehicles, high-strength low alloy TRIP-aided sheet steels associated with TRIP (TRansformation Induced Plasticity)[1] of retained austenite were applied for automotive parts due to excellent formabilities[2), 3), 4), 5), 6), 7)], impact properties[8)] and fatigue properties.[9), 10)] In the future, it is expected that ultra high-strength steels having a tensile strength more than 980 MPa grade will be required for auto motive parts since 590-980 MPa grade high-strength steels are used for present automotive high-strength sheet steels. Generally (1) deterioration of formabilities, (2) deterioration of impact properties and (3) occurrence of hydrogen embrittlement[11), 12)] are the problems when tensile strength exceeds 980 MPa. It has been reported that TRIP-aided bainitic ferrite steel with bainitic ferrite matrix (TBF steel) can exhibit excellent formability in the range of tensile strength more than 980 MPa because of TRIP effects of retained austenite.[4), 5)] On the other hand, impact properties of 980 MPa grade TBF steel were drastically deteriorated as shown in Fig. 1. In addition, hydrogen is expected to decrease toughness of TBF steels with tensile strength of more than 980 MPa grade, as occurs in conventional ultra high-strength steels.[11)]

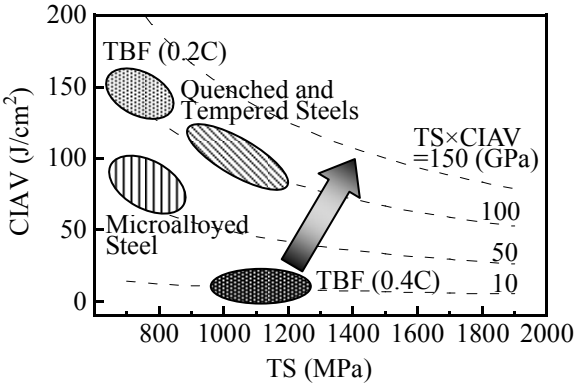

Fig. 1 Relationship between Charpy impact absorbed value (*CIAV*) and tensile strength (*TS*) of steels.

In general, impact properties and hydrogen embrittle-ment properties of TBF steels depend on microstructural morphology and characteristics of retained austenite. Since it has been reported that addition of alloying elements to TBF steel achieves fine microstructure and excellent retained austenite characteristics,[13), 14)] it is considered that impact properties and hydrogen embrittle-ment properties of TBF steels are improved by the addition of alloying elements.

In this study, to develop the ultra high-strength low alloy TRIP-aided sheet steel having excellent impact properties and hydrogen embrittlement properties, the effects of alloying elements and hydrogen charging on impact properties of ultra high-strength TBF steels have been investigated.

2. EXPERIMENTAL PROCEDURE

In this study, two kinds of vacuum melted and hot-forged slabs were prepared. Steel A is base steel with

Received 31. 8. 2010

* Department of Mechanical Engineering

** Graduate Student, Shinshu Unversity

*** Department of Mechanical System Engineering, Shinshu University

Table 1 Chemical composition (mass%) and estimated martensite-start temperature (M_S: °C) of steels.

Steel	C	Si	Mn	Al	Nb	Mo	Cr	M_S
A	0.40	1.47	1.50	0.04	-	-	-	348
B	0.40	0.49	1.48	0.96	0.024	0.10	-	376
M	0.39	0.19	0.68	0.031	-	0.17	0.95	383

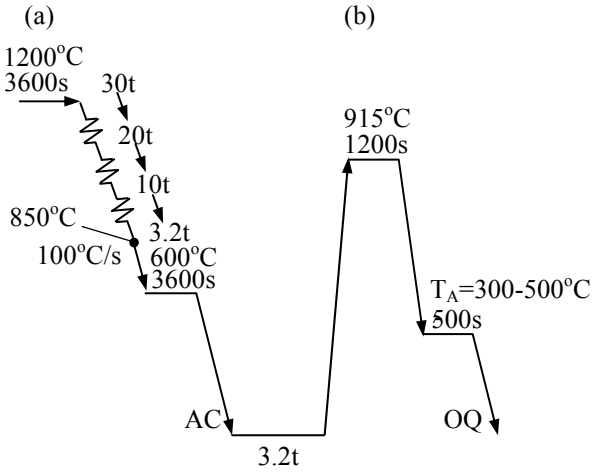

Fig. 2 Hot-rolling and heat treatment process of TBF steels.

chemical composition of 0.40 %C-1.47 %Si-1.50 %Mn. Steel B has additional aluminium of 0.96 %, niobium of 0.024 % and molybdenum of 0.10 %. Chemical compositions of these steels are listed in Table 1, with martensite-start temperature (M_S) estimated by the following equation (1).[15)]

$$M_S\,(^{o}C)=550-361\times(\%C)-39\times(\%Mn)-17\times(\%V)-20\times(\%Cr)-17\times(\%Ni)-10\times(\%Cu)-5\times(\%Mo+\%W)-0\times(\%Si)+15\times(\%Co)+30\times(\%Al) \quad (1)$$

where %X is content of element X in mass percent, respectively.

Hot-rolling process and heat treatment diagram are illustrated in Fig. 2 schematically. First, slabs were heated to 1200°C and hot-rolled to 3.2 mm thickness to a finishing rolling temperature of 850°C. Next, the sheet steels were annealed at 915°C for 1200 s in austenitic region and then austempered at 300-500°C for 500 s in salt baths to make the TBF steels. For comparison, tempered martensitic steel (M steel) was prepared by quenching and tempering at 200-600°C for 3600 s from commercial M steels (SCM435).

The volume fraction of retained austenite (f_γ, vol%) was quantified from the integrated intensity of (200)α, (211)α, (200)γ, (220)γ and (311)γ peaks by X-ray diffractometry using Mo-Kα radiation.[16)] The carbon concentration (C_γ, mass%) of retained austenite was estimated from the lattice parameter using equation (2). In this case, lattice constant (a_γ) was measured from (200)γ, (220)γ and (311)γ peaks of Cu-Kα radiation.[17)]

$$a_\gamma=3.5780+0.0330\times(\%C_\gamma)+0.00095\times(\%Mn_\gamma)+0.0\times(\%Si_\gamma)-0.0002\times(\%Ni_\gamma)+0.0006\times(\%Cr_\gamma)+0.0220\times(\%N_\gamma)+0.0056\times(\%Al_\gamma)-0.0004\times(\%Co_\gamma)+0.0015\times(\%Cu_\gamma)+0.0031\times(\%Mo_\gamma)+0.0079\times(\%Nb_\gamma)+0.0032\times(\%Ti_\gamma)+0.0017\times(\%V_\gamma)+0.0057\times(\%W_\gamma) \quad (2)$$

where concentrations of individual elements ($\%X_\gamma$) in retained austenite are in mass%, respectively. For convenience, added contents of alloying elements were substituted for these concentrations in this study.

Tensile tests were carried out on a hard type of testing machine at 25°C and at a crosshead speed of 1 mm/min (i.e. strain rate of 8.33×10^{-4} /s), using tensile specimens of 22 mm in gauge length, 4 mm in width and 2.5 mm in thickness. Tensile properties were evaluated by tensile strength (*TS*), 0.2 % offset proof stress (*YS*), total elongation (*TEl*), uniform elongation (*UEl*) and reduction of area (*RA*).

Impact tests were conducted on Charpy impact testing machine at a temperature range between -196 and 150°C before or after hydrogen charging using impact specimen of 55 mm in length, 10 mm in height and 2.5 mm in width with V- and U-notch. Liquid nitrogen, dry ice and ethanol were used for cooling the specimen. A thermostat bath was used when the specimen was heated. The specimens were held for 1800 s at the testing temperature before impact testing. Impact properties were evaluated by upper shelf Charpy impact absorbed value (*CIAV*) and fracture appearance transition temperature (*FATT*).

Hydrogen was charged in the 0.1 mass%KSCN solution (relative amount of solution=0.5 ml/mm^2) at 50°C for 48 hours. Total amount of solute hydrogen was measured by TCD (Thermal Conduction Detector). Specimen charged hydrogen was kept in liquid nitrogen to prevent hydrogen evolution from the specimen.

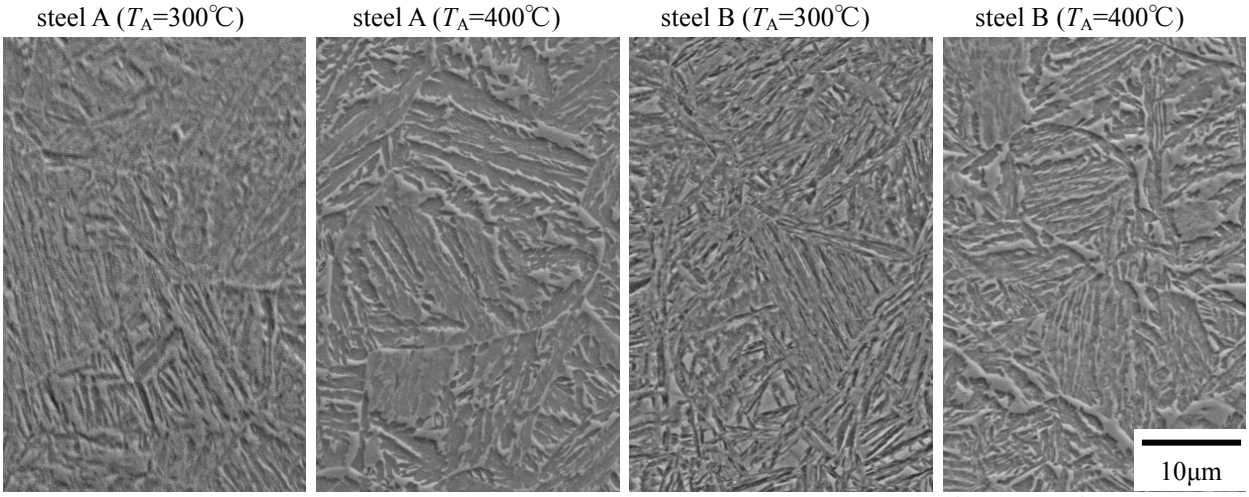

Fig. 3 Typical scanning electron micrographs of TBF steels austempered at 300°C and 400 °C.

Table 2 Tensile properties and retained austenite characteristics of TBF and M steels.

steel	T_A	*YS*	*TS*	*TEl*	*UEl*	$f_{\gamma 0}$	$C_{\gamma 0}$
A	300	1683	1833	10.6	3.8	7.8	0.48
	325	1464	1701	16.8	6.0	7.7	0.99
	350	1323	1515	15.7	6.1	11.6	1.26
	375	1132	1346	25.0	12.6	16.3	1.29
	400	948	1211	31.6	23.8	21.4	1.21
	425	756	1174	31.7	26.1	17.5	1.03
	450	732	1145	22.1	16.5	11.6	0.99
	475	694	1138	17.1	13.9	6.5	0.98
	500	699	1142	15.6	12.6	4.5	0.51
B	300	1538	1729	14.4	4.9	8.2	0.83
	325	1456	1604	15.5	4.7	13.8	1.12
	350	1297	1421	16.3	5.1	18.3	1.45
	375	1114	1246	18.8	7.2	20.2	1.61
	400	967	1083	28.5	14.8	23.5	1.47
	425	796	1007	40.5	32.4	30.0	1.38
	450	738	1026	41.4	34.2	26.0	1.24
	475	504	1109	29.4	24.2	33.7	1.16
	500	640	1101	22.4	15.5	14.0	0.84
M	200	1394	1915	24.3	20.8	-	-
	400	1209	1492	14.7	12.1	-	-
	600	917	1027	16.2	10.9	-	-

T_A(°C): austempering temperature, *YS* (MPa): yield stress or 0.2% offset proof stress, *TS* (MPa): tensile strength, *TEl* (%): total elongation, *UEl* (%): uniform elongation, $f_{\gamma 0}$ (vol%): initial volume fraction of γ_R, $C_{\gamma 0}$ (mass%): initial carbon concentration of γ_R

Table 3 Fracture appearance transition temperature (*FATT*) of TBF steels.

steel	A		B	
T_A (°C)	300	400	300	400
FATT (°C)	-2	33	-50	-33

3. RESULTS

3.1 MICROSTRUCTURE AND TENSILE PROPERTIES

Fig. 3 shows typical scanning electron micrographs of as heat treated TBF steels austempered at 300 and 400°C. Microstructures of these TBF steels consist of bainitic ferrite (α_{bf}) lath which has high dislocation density and interlath retained austenite (γ_R) films. When TBF steels are austempered below M_S, martensite (α_m) laths coexist with α_{bf}. In this case, volume fraction of the α_m increases with decreasing austempering temperature. Combined addition of Al-Nb-Mo tends to refine these lath width and retained austenite films and small prior austenite grain size in steel B.

Tensile properties and retained austenite characteristics of TBF and M steels after heat treatment are shown in Table 2. Initial volume fractions of retained austenite ($f_{\gamma 0}$) of steel A are between 4.5 and 21.4 vol%, and their carbon concentrations ($C_{\gamma 0}$) are between 0.48 and 1.29 mass% respectively. On the other hand, in steel B, $f_{\gamma 0}$ are between 8.2 and 33.7 vol% and their $C_{\gamma 0}$ are between 0.83 and 1.61 mass% respectively. Both $f_{\gamma 0}$ and $C_{\gamma 0}$ are increased by combined addition of Al-Nb-Mo.

Tensile strength (*TS*) of these steels are between 1101 and 1883 MPa and decrease with decreasing austempering temperature. The total elongations (*TEl*) are between 10.6 and 41.4 %. *TEl* of steel A are increased when steels A are austempered at 400 and 425°C. On the other hand, steels B austempering at 425-450°C indicate large *TEl* although *TS* of steel B are decreased compared with those of steel A.

3.2 IMPACT PROPERTIES

Fig. 4 shows Charpy impact absorbed value (*CIAV*) - testing temperature (*T*) curves for steels A, B and M for V- and U-notched specimens. When austempering treatments are carried out at 400°C for every TBF steels, upper shelf *CIAV* are higher than those of TBF steels austempered at 300°C. At austempering temperature of 400°C, steel B has higher *CIAV* compared to steel A at all tested temperatures, especially above -100°C. Table 3 shows fracture appearance transition temperature (*FATT*)

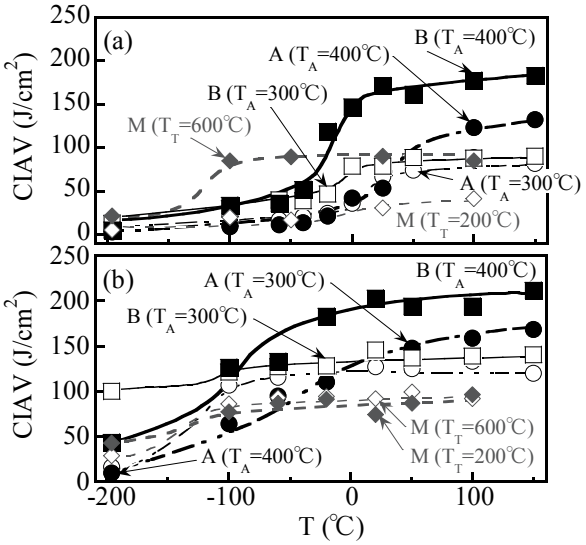

Fig. 4 Charpy impact absorbed value (*CIAV*) - testing temperature (*T*) curves for steels A, B and M for (a) V- and (b) U-notched specimens.

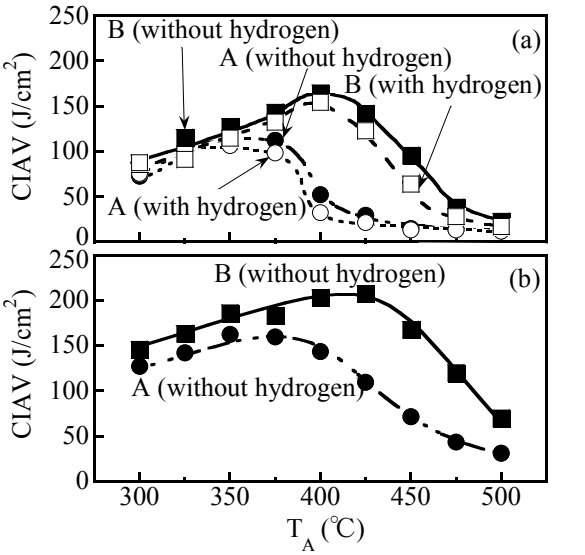

Fig. 5 Variations in Charpy impact absorbed value (*CIAV*) as a function of austempering temperature (T_A) in steels A and B testing at 25°C before and after hydrogen charging for (a) V- and (b) U-notched specimens.

of TBF steels. *FATT* of these TBF steels austempered at 300°C are lower than those of TBF steels austempered at 400°C. *FATT* of steel B tends to low temperature compared with that of steel A.

Fig. 5 shows variations in Charpy impact absorbed value (*CIAV*) as a function of austempering temperature (T_A) in TBF steels testing at 25°C before and after hydrogen charging for V- and U-notched specimens. The relationship between *CIAV* and tensile strength (*TS*) in TBF and M steels testing at 25°C before and after hydrogen charging for V- and U-notched specimens is shown in Fig. 6. It is found that *CIAV* of TBF steel is increased by combined addition of Al-Nb-Mo. *CIAV* of steels A and B drastically change with changing T_A.

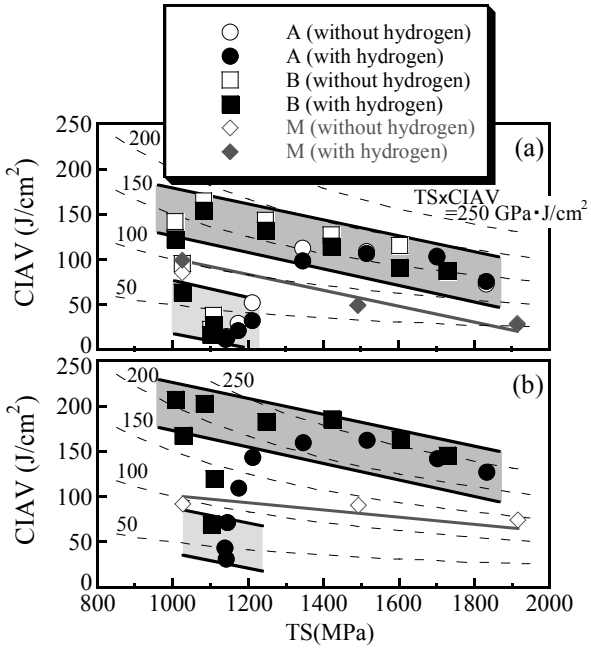

Fig. 6 Relationships between Charpy impact absorbed value (*CIAV*) and tensile strength (*TS*) in steels A, B and M testing at 25°C before and after hydrogen charging for (a) V- and (b) U-notched specimens.

Particularly, high *CIAV* suggests at the austempering temperature between 350 and 375°C in steel A. On the other hand, steel B combined added Al-Nb-Mo austempered between 375 and 425°C indicates high *CIAV*. When hydrogen is charged in TBF steels, the *CIAV* is slightly decreased. From Fig. 6, *CIAV* of TBF steel decreases with increasing the *TS*. When *CIAV* is arranged by the *TS*, *CIAV* bands which are higher and lower than that of steel M are appeared.

Fig. 7 shows scanning electron micrographs of fracture surface of steels A austempered at 300 and 400°C, B austempered at 300 and 400°C and M tempered at 600°C tested at -100 and 25°C (before and after hydrogen charging) for V-notched specimens. It is found that in the TBF steel tested at -100°C, fracture occurs by quasi cleavage. When impact test is conducted at 25°C without hydrogen, both dimple and quasi cleavage fracture occurre in steel A austempered at 300°C. In steel A austempered at 400°C, quasi cleavage fracture occurs as for at -100°C. On the other hand, dimple and quasi cleavage fracture coexist in the fracture surface of steel B austempered at 300°C. In steel B austempered at 400°C, fracture surface changes from quasi cleavage to dimple fracture. When TBF steel absorbs hydrogen, steel A austempered at 300°C and steel B austempered at 300 and 400°C indicate dimple fracture although dimple morphology becomes slightly large diameter compared with none hydrogen charged fracture surface. Steel A austempered at 400°C indicates quasi cleavage fracture

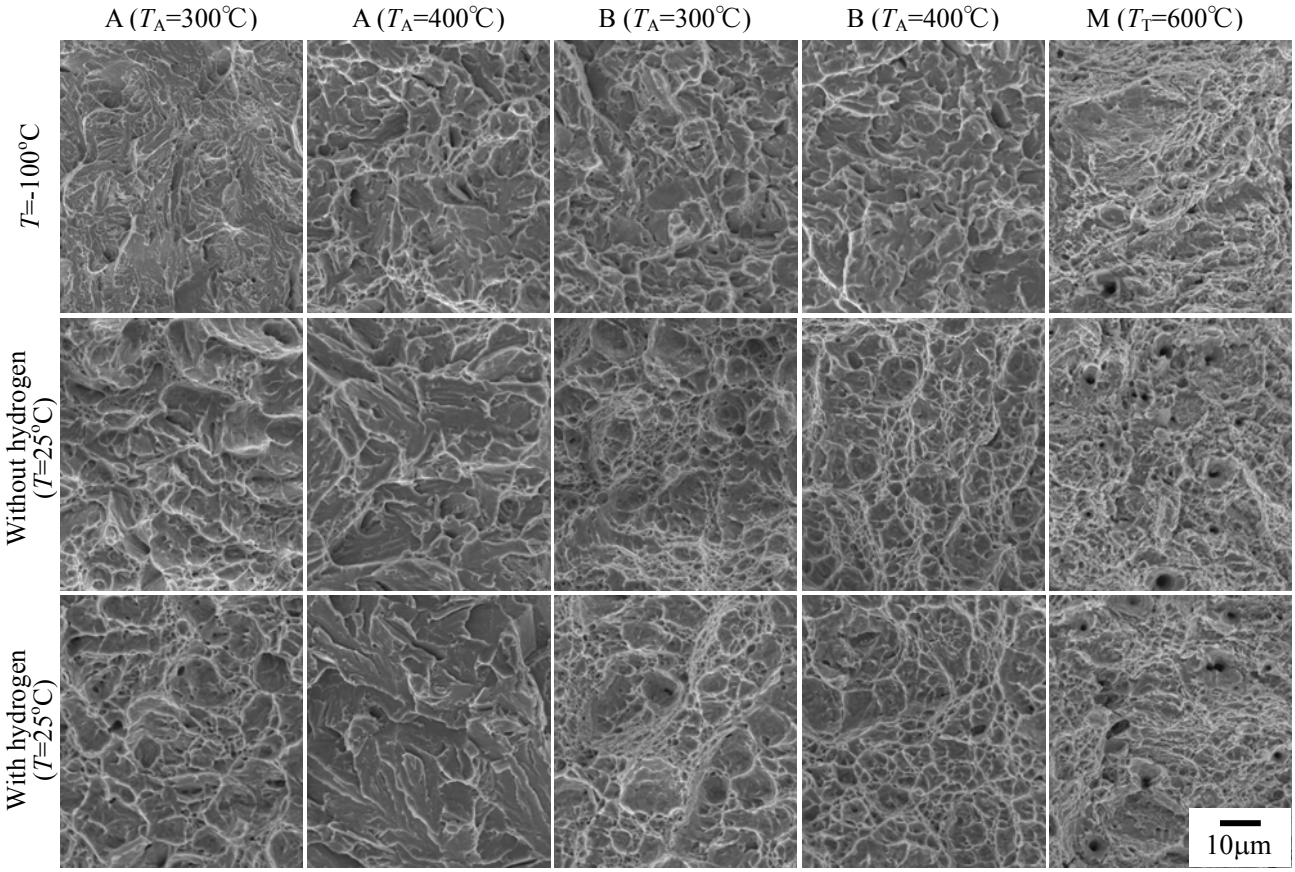

Fig. 7 Scanning electron micrographs of fracture surface of Steels A (T_A=300, 400°C), B (T_A=300, 400°C) and M (T_T=600°C) tested at -100 and 25°C (before and after hydrogen charging) for V-notched specimens.

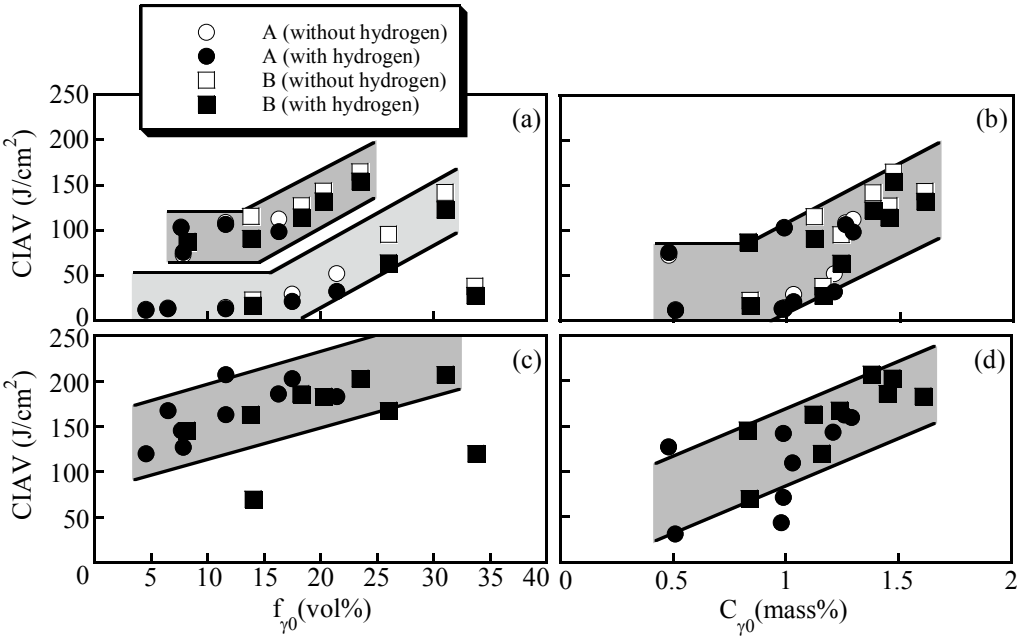

Fig. 8 Relationships between Charpy impact absorbed value (*CIAV*) and (a, c) initial volume fraction of γ_R ($f_{\gamma 0}$) and (b, d) initial carbon concentration of γ_R ($C_{\gamma 0}$) in steels A and B. (a, b) correspond to V-notched specimens and (c, d) to U-notched specimens.

as same as without hydrogen.

The tendency of impact properties between V- and U-notched specimens is similar in this study.

4. DISCUSION

4.1 EFFECTS OF HEAT TREATMENTS

Charpy impact absorbed values were changed by the different austempering temperature in TBF steels, especially, when austempering treatments were carried

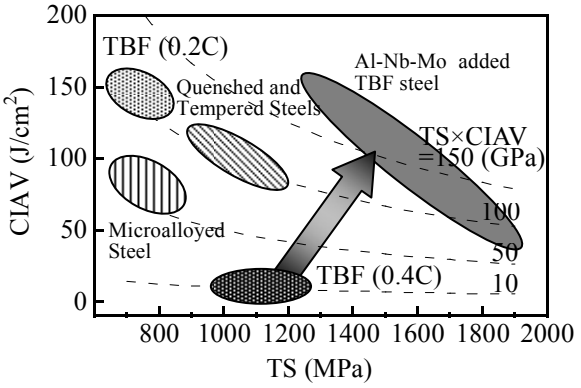

Fig. 9 Relationship between Charpy impact absorbed value (*CIAV*) and tensile strength (*TS*) of steels.

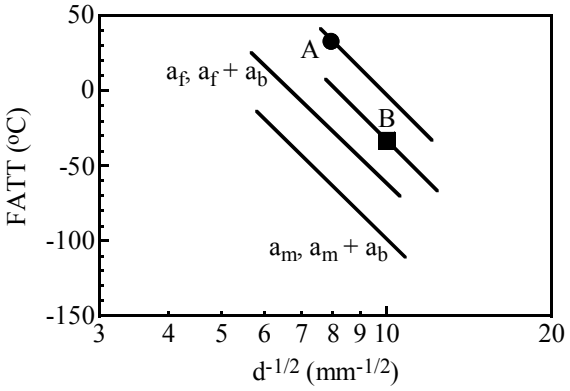

Fig. 10 Relationship between fracture appearance transition temperature (*FATT*) and unit crack path ($d^{-1/2}$) in steels A and B austempered at 400°C.

out at 350-375°C in steel A and 375-425°C in steel B. Fig. 8 shows relationships between initial volume fraction of retained austenite ($f_{\gamma 0}$) and its carbon concentration ($C_{\gamma 0}$) and Charpy impact absorbed value (*CIAV*) of TBF steels for V- and U-notched specimens. *CIAV* of every TBF steels are increased with increasing $f_{\gamma 0}$ and $C_{\gamma 0}$. It was expected that *CIAV* were related with retained austenite characteristics strongly. In these TBF steels, the retained austenite characteristics were drastically changed due to different austempering treatment for TBF steel (Table 2). According to previous studies,[4), 5), 13)] high- and ultra high-strength TRIP-aided steels obtain high $f_{\gamma 0}$ and $C_{\gamma 0}$ when austempering treatment is conducted just above the M_S. The M_S calculated by equation (1) of steel B was higher than that of steel A because M_S were 348°C for steel A and 376°C for steel B. Hence it was suggested that steel B indicated excellent retained austenite characteristics at higher T_A range than those of steel A. The retained austenite which has high carbon concentration suppressed the initiation and growth of voids due to an effective deformation induced martensite transformation.[8)] So it was noted that TBF steel which has high $f_{\gamma 0}$ and $C_{\gamma 0}$ indicated excellent *CIAV*.

When *CIAV* was arranged by the *TS*, there were two bands (i. e. high and low *CIAV* bands) (Fig. 6). TBF steels with the low *CIAV* were mainly austempered at the higher temperature. Microstructures of these steels were characterised by coarse bainitic ferrite morphology and blocky retained austenite. In addition, $f_{\gamma 0}$ and $C_{\gamma 0}$ were decreased at the high austempering temperature region. Thus it was considered that coarse lath morphology and deterioration of retained austenite characteristics brought the low *CIAV* in TBF steels.

4.2 EFFECTS OF ALLOYING ELEMENTS

In this study, high strength-toughness (*TS*-*CIAV*) balance of TBF steel compared with 590-780 MPa grade TBF steels and conventional quenched and tempered steels was achieved by combined addition of Al-Nb-Mo (Fig. 9). The volume fraction of retained austenite ($f_{\gamma 0}$) and its carbon concentration ($C_{\gamma 0}$) were higher in steel B than those of base steel (Table 2). Generally aluminium addition hardly changes the volume fraction of retained austenite, but promotes carbon-enrichment in retained austenite if austempering treatment is employed after annealing, because aluminium accelerates the start of ferrite transformation[18)] and increases T_0 temperature which inspires the concentration of carbon to retained austenite during austempering treatment.[13)] Thus it was considered that large amount of stable retained austenite was existed in steel B. As mentioned above, TBF steels which had high $f_{\gamma 0}$ and $C_{\gamma 0}$ indicated excellent *CIAV* (Fig. 8). Moreover, microstructure of Al-Nb-Mo combined added TBF steel was refined bainitic ferrite lath morphology and small prior austenite grain size as shown in Fig. 3. It is known that voids and cracks of conventional steels initiate at grain boundary, lath boundary, matrix/carbide boundary and matrix/second phase boundary, and the cracks propagate along the grain and lath boundaries. In the fracture surface, steel B showed smaller size of dimple than steel A. This dimple size corresponded with bainitic ferrite lath width. So it was noted that initiation of voids in TBF steel was mainly at the lath boundaries. In addition, retained austenite of steel B was distributed finer and more uniformly at the lath boundaries than that of steel A. It was suggested that if the voids occurred at the bainitic ferrite lath boundary, growth of voids was suppressed by a stress relaxation of deformation induced by transformation of this fine retained austenite. So it has been considered that TBF steel with combined addition of Al-Nb-Mo obtained high *CIAV* compared with base steel due to the suppression of initiation and growth of voids because of (1) existence of large amount of stable retained austenite and (2) the refine and the uniform of microstructure.

On the other hand, the fracture appearance transition temperature (*FATT*) of TBF steel decreased by a combined addition of Al-Nb-Mo (Table 3). Generally, relationship between *FATT* and unit crack path (*d*) is given by following equation (3).[19]

$$FATT \propto d^{-1/2} \quad (3)$$

Fig. 10 shows relationship *FATT* and unit crack path ($d^{-1/2}$) in steels A and B austempered at 400°C. For the reference, results of ferrite-bainaite or bainitic and martensite-bainite or martensitic steels which don't include the retained austenite are shown in this figure.[19] *FATT* of TBF steels decreased with increasing $d^{-1/2}$. As mentioned above, the prior austenite grain size of TBF steel was smaller by the combined addition of Al-Nb-Mo due to a precipitation of carbide such as NbC during hot-rolling process. Furthermore, Al-Nb-Mo combined addition to the TBF steel leaded to refined bainitic ferrite morphology. These mcrostructure changes may be lower the *FATT* of steel B than that of base steel.

4.3 EFFECTS OF HYDROGEN

In this study, Charpy impact absorbed value of TBF steel has not been deteriorated by absorption of hydrogen. Total hydrogen concentration (H_T) of TBF steels after hydrogen charging is shown in Fig. 11. TBF steels absorbed hydrogen more than 1 ppm. Particularly, the H_T of steel B austempered more than 375°C was increased. Fig. 12 shows relationship between total hydrogen concentration (H_T) and initial volume fraction of retained austenite ($f_{\gamma 0}$) of TBF steels. It was found that H_T of TBF steel was increased with increasing $f_{\gamma 0}$. Chan *et al.*[20] have reported that martensitic steels containing retained austenite absorbed more hydrogen than martensitic steels without retained austenite, and this result was caused by a great deal of hydrogen trapping at retained austenite/martensite interface. In this study, a large amount of retained austenite existed in the TBF steel. Therefore, it was suggested that a lot of hydrogen was trapped in the retained austenite and/or at the bainitic ferrite matirix/retained austenite interface. In conventional ultra high-strength steel, hydrogen is mainly trapped on the grain boundaries,[21] on dislocations[22] and at carbide/matrix interfaces.[21), 23] Hydrogen trapped at grain boundaries reduces atomic binding energy of the boundaries, and makes crack propagation along it easier.[11] However, in TBF steel, it was expected that hydrogen trapping to at the grain and lath boundaries was suppressed because of a large amount of hydrogen trapping in the retained austenite and at the matrix/retained austenite interface. From Fig. 7, there was small change in the fracture surface of TBF steel although TBF steel charged hydrogen more than 1 ppm. Thus, it was note that since TBF steel suppressed the hydrogen trapping to the grain and lath boundaries due to the high hydrogen absorption capacity of retained austenite, deterioration of *CIAV* of TBF steel was small.

Fig. 13 shows relationship between reductions of Charpy impact absorbed value (*CIAV*) after hydrogen charging and total hydrogen concentration (H_T) of steels A and B. It was found that amounts of reduction of *CIAV*

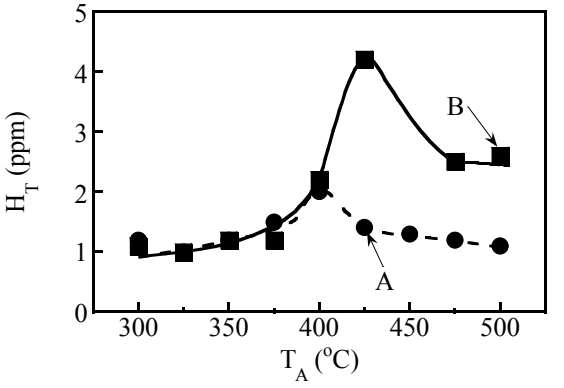

Fig. 11 Variations in total hydrogen concentration (H_T) as a function of austempering temperature (T_A) in steels A and B.

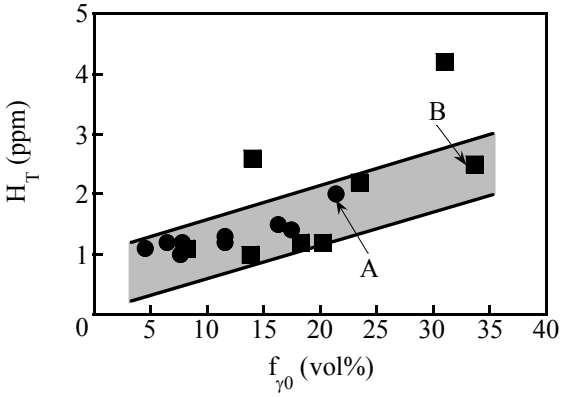

Fig. 12 Relationship between total hydrogen concentration (H_T) and initial volume fraction of γ_R ($f_{\gamma 0}$) of TBF steels.

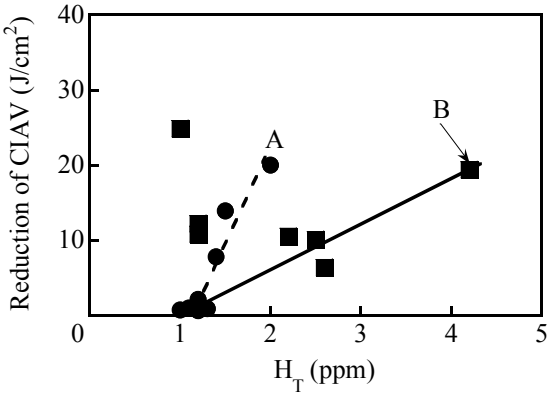

Fig. 13 Relationship between reductions of Charpy impact absorbed value (*CIAV*) after hydrogen charging and total hydrogen concentration (H_T) of TBF steels.

of every TBF steels were increased with increasing the H_T. However, if H_T was increased, amount of reduction of *CIAV* of steel B did not increase as much as that of steel A. As mentioned above, a large amount of hydrogen was trapped in retained austenite and at matrix/retained austenite interface. TBF steel with addition of Al-Nb-Mo indicated higher $f_{\gamma 0}$ than steel A (Table 2). It was considered that the effects of H_T on the reduction of *CIAV* were small because of the existence of a large amount of retained austenite in steel B.

5. CONCLUSIONS

The effects of alloying elements on impact properties and hydrogen embrittlement properties of ultra high-strength TRIP-aided bainitic ferrite steel was investigated to apply the ultra high-strength low alloy TRIP-aided steel for automotive structural steel. The results are summarised as follows.

(1) C-Si-Mn TBF steel austempered at 350-375^{o}C and C-Si-Mn-Al-Nb-Mo TBF steel austempered at 375-425^{o}C indicated high Charpy impact absorbed value. This was caused by the high initial volume fraction of retained austenite and its carbon concentration in those austempering temperatures.

(2) Al-Nb-Mo combined addition increased the Charpy impact absorbed value and lower the fracture appearance temperature of TBF steels. Increase in the impact absorbed value of Al-Nb-Mo TBF steel may be due to the increase in the initial volume fraction of retained austenite and its carbon concentration. The decrease in the fracture appearance transition temperature by the combined addition of Al-Nb-Mo was caused by the refine and uniform bainitic ferrite lath matrix and small grain size.

(3) Charpy impact absorbed value of TBF steels was hardly decreased by hydrogen charging compared with that of TBF steel without hydrogen. This was consistent with reduction of hydrogen at the grain and lath boundaries due to the hydrogen trapping in the retained austenite and/or at the matrix/retained austenite interface.

ACKNOWLEDGEMENTS

The authors gratefully acknowledge financial support by Okayama Industrial Promotion Foundation and Electric Technology Research Foundation of Chugoku.

REFERENCES

1) V. F. Zackay, E. R. Parker, D. Fahr and R. Bush: The Enhancement of Ductility in High-Strength Steels, *Trans. Am. Soc. Met.*, **60** (1967), 252-259.
2) K. Sugimoto, M. Kobayashi and S. Hashimoto: Ductility and Strain-Induced Transformation in a High-Strength Transformation -Induced Plasticity-Aided Dual-Phase Steel, *Metall. Trans. A*, **23A** (1992), 3085-3091.
3) O. Matsumura, Y. Sakuma, Y. Ishii and J. Zhao: Effect of Retained Austenite on Formability of High Strength Sheet Steels, *ISIJ Int*., **32** (1992), 1110-1116.
4) K. Sugimoto, J. Sakaguchi, T. Iida and T. Kashima: Stretch -Flangeability of a High-Strength TRIP Type Bainitic Sheet Steel, *ISIJ Int*., **40** (2000), 920-926.
5) K. Sugimoto, M. Tsunezawa, T. Hojo and S. Ikeda: Ductility of 0.1-0.6C-1.5Si-1.5Mn Ultra High-Strength TRIP-Aided Sheet Steels with Bainitic Ferrite Matrix, *ISIJ Int*., **44** (2004), 1608-1614.
6) K. Sugimoto, R. Kikuchi, M. Tsunezawa, S. Hashimoto, T. Kashima and S. Ikeda: The Effects of Heat Treatment Conditions on Stretch-Flangeability and Bendability of High-Strength Low Alloy TRIP-Aided Sheet Steels with Annealed Martensitic Matrix, *Tetsu-to-Hagane*, **89** (2003), 1065-1070.
7) K. Sugimoto, A. Kanda, R. Kikuchi, S. Hashimoto, T. Kashima and S. Ikeda: Ductility and Formability of Newly Developed High Strength Low Alloy TRIP-Aided Sheet Steels with Annealed Martensite Matrix, *ISIJ Int*., **42** (2002), 910-915.
8) S. Song, K. Sugimoto, M. Kobayashi, H. Matsubara and T. Kashima: Impact Properties of Low Alloy TRIP Steels, *Tetsu-to-Hagane*, **86** (2000), 563-569.
9) K. Sugimoto, S. Song, K. Inoue, M. Kobayashi and S. Masuda: Effects of Prestraining on Low Cycle Fatigue Properties of Low Alloy TRIP Steels: *J. Soc. Mater. Sci., Jpn.*, **50** (2001), 657-664.
10) S. Song, K. Sugimoto, S. Kandaka, A. Futamura, M. Kobayashi and S. Masuda: Effects of Prestraining on High Cycle Fatigue Strength of High Strength Low Alloy TRIP Steels: *J. Soc. Mater. Sci., Jpn.*, **50** (2001), 1091-1097.
11) S. Matsuyama: Delayed Fracture, Nikkan Kogyo Shinbun Ltd., Tokyo, (1989).
12) H. Tsubakino, H. Harada: Effects of Retained Austenite on Hydrogen Permeation Behaviour in Steels, Advance in Delayed Fracture Solution, ISIJ, Tokyo (1997), 138-143.
13) K. Sugimoto, B. Yu, Y. Mukai and S. Ikeda: Microstructure and Formability of Aluminum Bearing TRIP-Aided Steels with Annealed Martensite Matrix, *ISIJ Int*., **45** (2005), 1194-1200.
14) M. Murata, J. Kobayashi and K. Sugimoto: Stretch-Flangeability of Ultra High-Strength Low Alloy TRIP-Aided Sheet Steels with Mixed Structure Matrix of Bainitic Ferrite and Martensite, *Bull. Iron Steel Inst. Jpn.*, **15** (2010), 84-92.
15) I. Tamura: Steel Material Study on the Strength, Nikkan Kogyo Shinbun Ltd., Tokyo, (1970), 40.
16) H. Maruyama: X-Ray Measurement of Retained Austenite Volume Fraction, *J. Jpn. Soc. Heat Treat*., **17** (1977), 198-204.
17) D. J. Dyson and B. Holmes: Effects of Alloying Elements on the Lattice Parameter of Austenite, *J. Iron Steel Inst.*, **208** (1970), 469-474.
18) W. Bleck, A. Frehn and J. Ohlert: Niobium in Dual Phase and TRIP Steels, Proc. of Int. Sympo. Niobium 2001, TMS, PA, (2001), 727-752.
19) H. Ohtani, F. Terasaki and T. Kunitake: The Microstructure and Toughness of High Tensile Strength Steels, *Tetsu-to-Hagane*, **58** (1972), 434-451.
20) S. L. I. Chan, H, L, Lee and J. R. Yang: Effect of Retained Austenite on the Hydrogen Content and Effective Diffusitivity of Martensitic Structure, *Metal. Trans. A*, 22A (1997), 2579-2586.
21) A. Kimura and H. Kimura: Effect of Carbon on the Hydrogen Induced Grain Boundary Fracture in Iron, *J. Jpn. Inst. Met.*, **47** (1983), 807-813.
22) T. Kushida: Correlation of Hydrogen Evolution Behaviour from Steel Observed by Thermal Desorption Analysis with Hydrogen Embrittlement, Advance in Delayed Fracture Solution, ISIJ, Tokyo (1997), 35-40.
23) T. Tsuchida, T. Hara and K. Tsuzaki: Relationship between Microstructure and Hydrogen Absorption Behavior in a V-bearing High Strength Steel, *Tetsu-to-Hagane*, **88** (2002), 771-778.